Geophysical Research Letters

RESEARCH LETTER
10.1029/2024GL110127

Geodynamic Evolution of the Lau Basin

Diandian Peng[1] and Dave R. Stegman[1]

[1]Institute of Geophysics and Planetary Physics, Scripps Institution of Oceanography, University of California, San Diego, CA, USA

Key Points:

- Trench retreat rate exerts primary control on the Tonga-Kermadec slab morphology and back arc basin formation
- Opening of the Lau Basin is dynamic with eastward migration of both the Tonga Ridge and Lau Ridge
- The South Fiji Basin experienced lithospheric thinning due to the fast mantle flow induced by the Tonga slab

Supporting Information:

Supporting Information may be found in the online version of this article.

Correspondence to:

D. Peng,
d3peng@ucsd.edu

Citation:

Peng, D., & Stegman, D. R. (2024). Geodynamic evolution of the Lau basin. *Geophysical Research Letters*, *51*, e2024GL110127. https://doi.org/10.1029/2024GL110127

Received 13 MAY 2024
Accepted 30 JUL 2024

Author Contributions:

Conceptualization: Diandian Peng, Dave R. Stegman
Data curation: Diandian Peng
Formal analysis: Diandian Peng
Funding acquisition: Dave R. Stegman
Investigation: Diandian Peng
Methodology: Diandian Peng, Dave R. Stegman
Project administration: Dave R. Stegman
Resources: Diandian Peng
Software: Diandian Peng
Supervision: Dave R. Stegman
Validation: Diandian Peng, Dave R. Stegman
Visualization: Diandian Peng
Writing – original draft: Diandian Peng
Writing – review & editing: Diandian Peng, Dave R. Stegman

Abstract The formation of Lau Basin records an extreme event of plate tectonics, with the associated Tonga trench exhibiting the fastest retreat in the world (16 cm/yr). Yet paleogeographic reconstructions suggest that seafloor spreading in the Lau Basin only initiated around 6 Ma. This kinematics is difficult to reconcile with our present understanding of how subduction drives plate motions. Using numerical models, we propose that eastward migration of the Lau Ridge concurrent with trench retreat explains both the narrow width and thickened crust of the Lau Basin. To match the slab geometry and basin width along the Tonga-Kermadec trench, our models suggest that fast trench retreat rate of 16 cm/yr might start ~15 Ma. Tonga slab rollback induced vigorous mantle flow underneath the South Fiji Basin which is driving the extension and thinning of the basin and contributing to its observed deeper bathymetry compared to neighboring basins.

Plain Language Summary The opening of the Lau Basin is complex. In this study, we used numerical models to examine the connection between Tonga subduction and the opening of the Lau Basin. Our models correctly predicted the observed slab structure and size of the Lau Basin. This challenges the current idea that the Lau Basin floor started spreading apart about 6 million years ago. We proposed a new theory. When the Tonga trench is retreating eastward, the Lau Ridge on its western boundary of the Lau Basin is moving toward the trench. This movement could explain the width of the Lau Basin width and the fact that its curst is thicker on the western side than the eastern side. We also suggest that the South Fiji Basin must have stretched and thinned during this process due to the vigorous flow induced by the Tonga slab rollback. The thinned crust making it deeper than nearby basins. The eastward movement of the Lau Ridge could also mean that the amount of trench retreat is larger than previously thought. This might require a revision of plate reconstruction in this region to account for the stretching in the South Fiji Basin.

1. Introduction

The southwestern Pacific is ideal for studying back-arc basin formation due to the presence of multiple basins at various stages of development (Figure 1a). The South Fiji Basin (SFB) exhibits no ongoing seafloor spreading, while active spreading characterizes the North Fiji Basin (NFB), Lau Basin, and Havre Trough. The SFB might form as a back-arc basin due to the Tonga-Kermadec subduction (Hall, 2002; Herzer et al., 2011; Sdrolias & Müller, 2006; Van De Lagemaat & Van Hinsbergen, 2024). The opening of the NFB is attributed to the retreat of the New Hebrides trench (Artemieva, 2023; Wallace et al., 2005). Similarly, the opening of the Lau Basin and Havre Trough may be a consequence of Tonga-Kermadec trench retreat (Bevis et al., 1995; Caratori Tontini et al., 2019; Gill, 1976) or potentially influenced by localized lateral mantle flow (Heuret & Lallemand, 2005).

Geomagnetic data and volcanic rocks provide the primary constraints on the ages of back-arc basins and ridges (Figure 1b). The SFB might form between ~35 Ma and ~15 Ma (Hall, 2002; Herzer et al., 2011; Sdrolias & Müller, 2006; Van De Lagemaat & Van Hinsbergen, 2024). The NFB initiated spreading ~12 Ma due to the New Hebrides subduction (Hall, 2002; Mann & Taira, 2004). The Lau Basin and Havre Trough are bounded on the west by the Lau-Colville Ridge, which was active at 14–2 Ma (Artemieva, 2023), and on the east by the active Tonga-Kermadec Ridge. These ridges were created as a single volcanic arc that subsequently rifted during Lau Basin and Havre Trough opening (Caratori Tontini et al., 2019; Gill, 1976). The rifting event is estimated to have begun around 10 Ma (Hall, 2002). Most studies place the onset of seafloor spreading and Lau Basin and Havre Trough formation around 6 Ma (Caratori Tontini et al., 2019; Mann & Taira, 2004; Ruellan et al., 2003; Sdrolias & Müller, 2006; Taylor et al., 1996). Although the ages of these back-arc basins are highly episodic, the age range for subduction-related arc volcanism appears continuous throughout this period (Mortimer et al., 2010). This discrepancy highlights a critical knowledge gap regarding the relationship between back-arc basin formation and the subduction history.

10.1029/2024GL110127

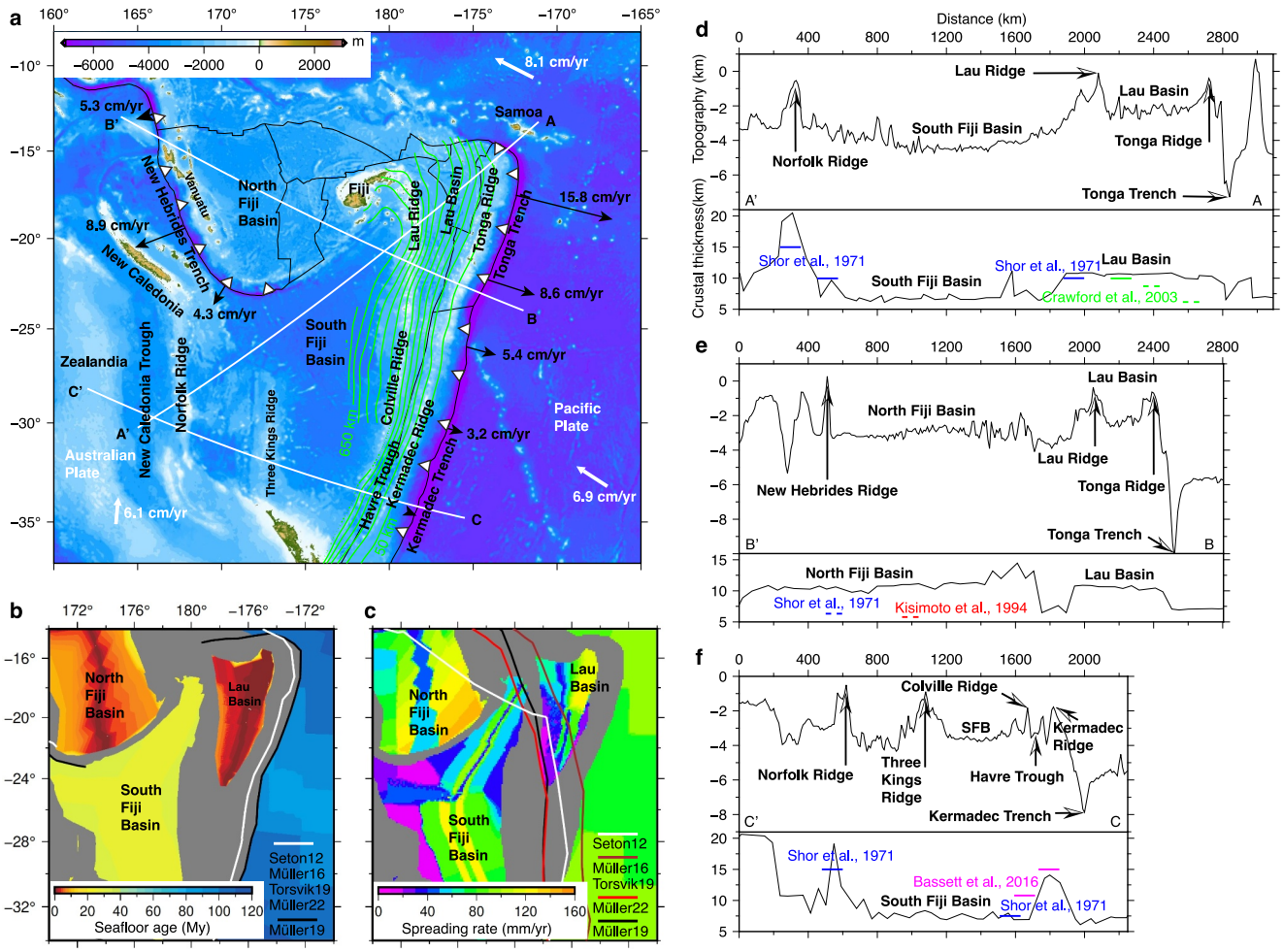

Figure 1. Geological background. (a) The topography with white arrows indicating plate motion and black arrows indicating trench migration rate (based on Schellart et al., 2007). The plate boundary is from Bird (2003). Green contours represent the Tonga slab depth based on slab2 (Hayes et al., 2018). White lines AA', BB', and CC' mark the cross-sections presented in (d, e, f). (b, c) Seafloor age and spreading rate according to Seton et al. (2020). The present-day trench locations are marked by white and black lines in (b). The locations of the trench at 15 Ma are depicted by white, brown, red, and black lines in (c), along with corresponding plate reconstructions (Müller et al., 2016, 2022; Seton et al., 2012; Torsvik et al., 2019). (d, e, f) The topography (upper panel) and crustal thickness based on Crust1.0 (lower panel) along AA', BB', and CC', respectively. Colored bars represent crustal thickness from corresponding references (solid bars at approximate locations and dashed bars for reference only).

Significant uncertainties remain regarding the opening pattern and spreading rate of the Lau Basin (Figure 1c). The opening may have occurred in distinct stages (Ruellan et al., 2003; Taylor et al., 1996), with the propagation along a single migrating spreading center (Parson et al., 1990) or simultaneous activities at multiple spreading centers (Stewart et al., 2022; Zellmer & Taylor, 2001). The Lau Basin exhibits highly asymmetric seafloor spreading with the ridge migrating toward the arc (Parson et al., 1990). This asymmetry is reflected in the variations of seafloor age and spreading rate across the basin (Figures 1b and 1c).

The crustal structure of the southwestern Pacific remains poorly constrained due to limited data availability (Artemieva, 2023). Crust 1.0 provides a first-order estimate, indicating a thickness of ~7 km in the center of the SFB (Figures 1d and 1f). Seismic refraction studies measured a thicker crust of 9.3 km for the SFB near its boundaries (Shor et al., 1971), consistent with Crust 1.0 (Figures 1d and 1f). The NFB exhibits a discrepancy with Crust 1.0 suggesting a 10 km thickness (Figure 1e), while seismic reflection/refraction data reveal a thinner crust (4–6.5 km) near its south end (Kisimoto et al., 1994; Shor et al., 1971). The thicker crust given by Crust 1.0 aligns better with the fact that NFB has higher topography than SFB. Crust 1.0 estimates a 11 km thick crust for the Lau Basin (Figures 1d and 1e). In contrast, seismic refraction data along a specific cross-section documented an westward thickening trend, with crustal thickness increasing from 5.5 to 6.5 km in the east to 7.5–8.3 km centrally

and reaching 9 km in the west (Crawford et al., 2003). The step of crustal thickness may correlate with the presence and migration of spreading centers within the Lau Basin. Seismic reflection/refraction data from the Havre Trough suggests a northward thinning crust, with the thickness ranging from up to 12 km in the north to 8–9 km centrally and 6–7 km in the south (Bassett et al., 2016; Caratori Tontini et al., 2019). All ridges in the region, including the Lau-Colville Ridge, Tonga-Kermadec Ridge, Three Kings Ridge, and Norfolk Ridge, exhibit thicker crust than the basins (Bassett et al., 2016; Caratori Tontini et al., 2019; Crawford et al., 2003; Kisimoto et al., 1994; Shor et al., 1971). A general positive correlation exists between topography and crustal thickness in regions with observational data, consistent with the theory of isostasy. This implies that poorly observed inner SFB might have thinner crust compared to the NFB, Lau Basin, and Havre Trough, which exhibit higher topography.

In this study we employ two-dimensional (2D) numerical models to investigate the geodynamic processes governing the subduction of the Tonga slab and the associated overriding plate deformation. Our primary focus is on elucidating the lithospheric evolution of the overriding plate, particularly the enigmatic opening of the Lau Basin. 2D numerical modeling offers a valuable tool for understanding these complex tectonic processes by allowing us to isolate key factors and explore large-scale deformation patterns.

2. Methods

We used two-dimensional (2D) mantle convection models in an equatorial slice of a sphere to investigate the subduction dynamics. Simulations were performed using CitcomS (McNamara & Zhong, 2004; Tan & Gurnis, 2007; Zhong et al., 2000), operating under a Boussinesq approximation. In the models, we used a visco-plastic rheology with diffusion creep in the lower mantle, diffusion and dislocation creep in the upper mantle (Billen & Hirth, 2007). Chemical tracers were used to track the migration of materials. Specific tracer flavors were defined to represent distinct lithological and tectonic units. They help to monitor the subducted slab and deformations within the overriding plate. Model details can be found in the Supporting Information S1 and Peng and Stegman (2024).

We implemented a hybrid velocity boundary condition on the overriding plate (Peng & Stegman, 2024). The Arc and Pacific Plate have imposed velocities, while the Australian Plate has a free slip surface. The Pacific Plate has a westward motion of 7 cm/yr (Figure S1 in Supporting Information S1). To investigate the influence of overriding plate dynamics, we tested two western boundary configurations: (a) Australian lithosphere extending to the boundary (fixed tail), and (b) a 600 km-wide ambient mantle zone on the western boundary, simulating a freely trailing overriding plate.

3. Results

The Lau Ridge was active at 14–2 Ma (Artemieva, 2023), which informs our decision to initiate models at 15 Ma. We present seven modeling cases designed to explore the following objectives. Cases 1–3: Investigate the impact of varying trench retreat rates on slab geometry. Cases 4–5: Test the hypothesis of temporally variable trench retreat rates. Cases 6–7: Assess the deformation and migration patterns of the Australian Plate under different kinematic conditions.

3.1. The Slab Geometries Along the Tonga-Kermadec Trench

The Tonga-Kermadec retreat rate decreases from north to south (Figure 1), being ∼16 cm/yr along cross-section AA', ∼8 cm/yr along BB', and ∼1 cm/yr along CC'. To investigate the impact of this spatial variation, we designed Cases 1, 2, and 3, each incorporating the respective trench retreat rates. These cases assume a fixed western edge for the Australian Plate.

The Tonga slab beneath AA' exhibits a distinctive morphology characterized by a kink around 400 km depth (Conder & Wiens, 2006; Peng & Stegman, 2024; Richards et al., 2011). This translates to a large dip angle from the surface to 400 km, followed by a segment of near-horizontal subduction (flat slab) and a subsequent resumption of a steep, near-vertical dip angle until encountering a flattened segment exceeding 1,000 km in length near the 670 km discontinuity (Figure 2a). The slab flattening near 670 km depth likely arises from the rapid trench retreat (Christensen, 1996; Peng & Stegman, 2024). Case 1, which incorporates a constant trench retreat

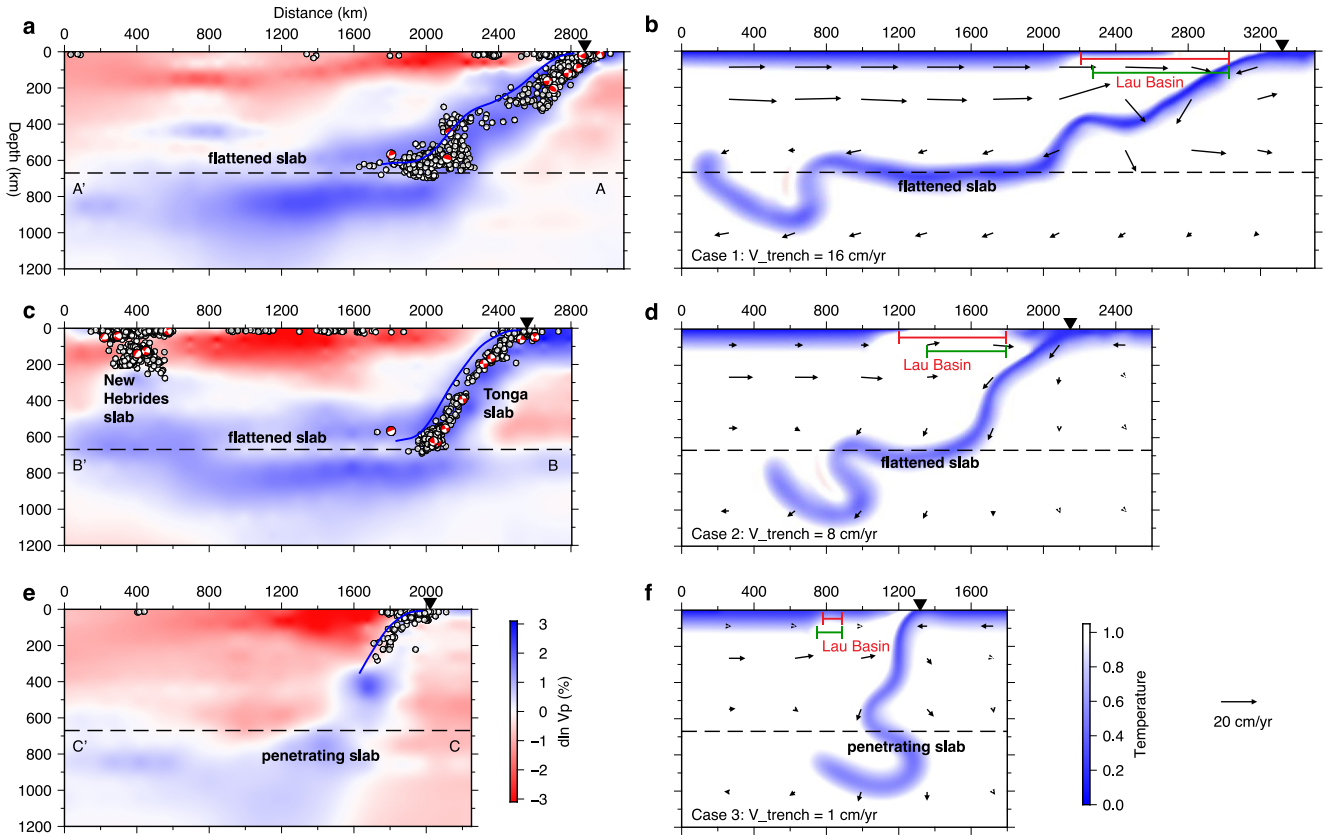

Figure 2. Comparing observed Tonga-Kermadec slabs with model results. (a, b) Case 1 captures the Tonga slab dip angle variations and the flattened slab near 670 km along AA' (see Movie S1 for the model evolution). (c, d) Case 2 yields a similar slab dip angle in the upper mantle but a shorter flattened slab compared to observations along BB'. This discrepancy is due to the absence of the New Hebrides slab in our model. (e, f) The model successfully replicates the penetrating slab morphology and possibly the curvature seen in the observed slab along cross-section CC'. The tomography model is GAP-P4 (Obayashi et al., 2013). Earthquake epicenters from the Global CMT (Ekström et al., 2012) are plotted as beach balls. The Tonga slab surface, derived from slab2, is outlined in blue. The black triangles mark the trench locations. The red and green bars in (b, d, f) represent the modeled and observed Lau Basin width, respectively.

rate of 16 cm/yr, successfully reproduces this variation in slab dip angle with depth (Figure 2b). Notably, the model predicts a Lau Basin width of ~700 km, which closely matches observations (Figure 2b).

Along cross-section BB', the observed slab dip is smoother with a consistently large angle from the surface to the 670 km discontinuity, where a flattened slab segment is present (Figure 2c). With a constant trench retreat rate of 8 cm/yr, Case 2 partially reproduces this geometry in the upper mantle. However, the modeled flattened slab is shorter than that observed in GAP-P4. This discrepancy can be attributed to the fact that our model focuses solely on the Tonga slab, while BB' intersects two subduction zones. The New Hebrides slab is not included in Case 2. The width of modeled Lau Basin width, 600 km, is slightly larger than the observed extent (Figure 2d).

Cross-section CC' reveals that the Kermadec slab penetrates directly into the lower mantle (Figure 2e). The slab in the lower mantle curves back. Case 3 successfully replicates the penetrating slab and partially captures the curvature observed in GAP-P4 (Figure 2f). However, a key difference exists: the modeled slab bends eastward within the mantle transition zone, whereas the observed curvature trends eastward. The model successfully predicts a narrow Havre Trough at ~100 km (Figure 2f).

These results demonstrate a compelling correlation between the trench retreat and slab geometry. This suggests that the trench retreat rate exerts a primary control on both slab geometry and the width of the back arc basins along the Tonga-Kermadec trench system.

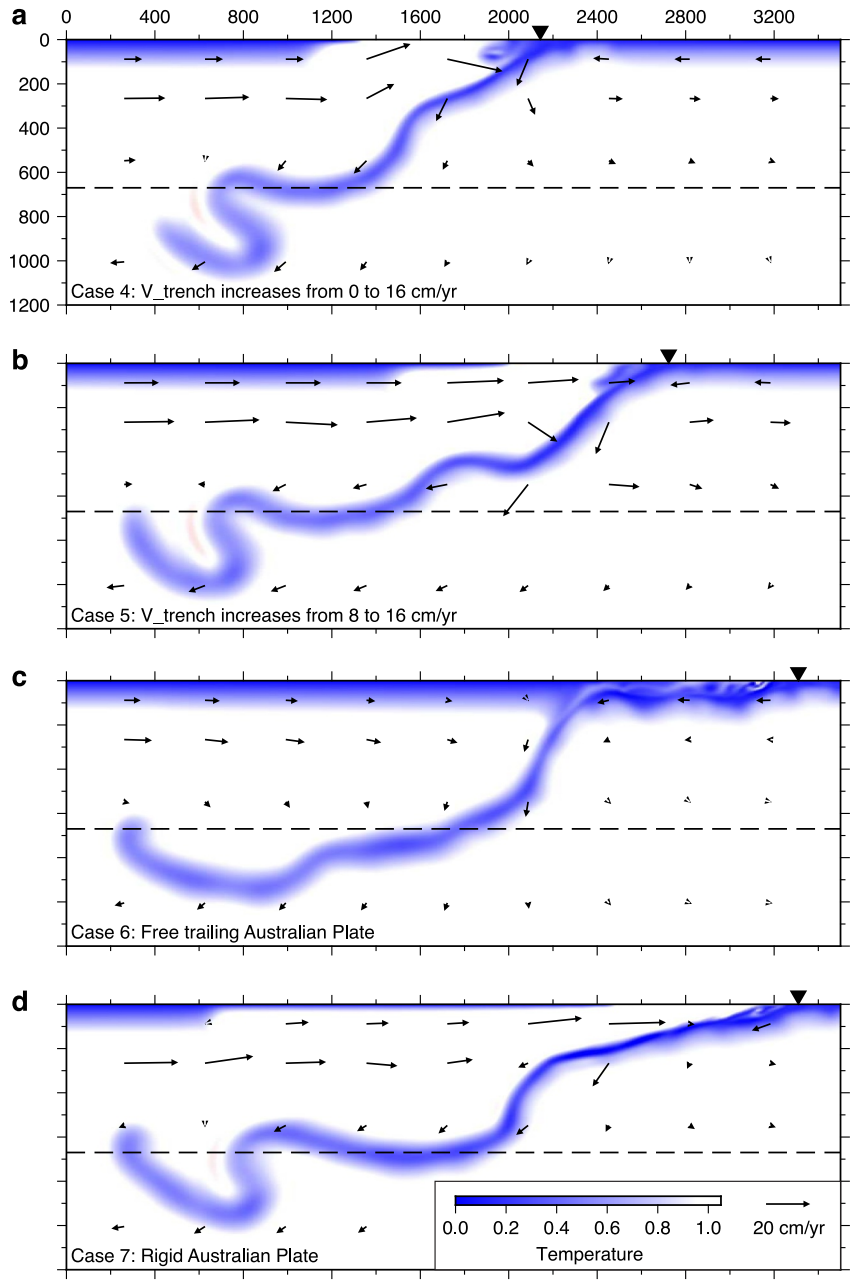

Figure 3. Investigating the impact of trench retreat rate and overriding plate dynamics. (a) Case 4 has a trench retreat rate that increases from 0 cm/yr at 15 Ma to 16 cm/yr at present. (b) Case 5 has a retreat rate rising from a 8 cm/yr at 15 Ma to 16 cm/yr at present. (c) Case 6 has a free-trailing Australian Plate which exhibits significant eastward movement of the plate. (d) Case 7 features a rigid, non-deformable Australian Plate.

3.2. The Impact of Time-Varying Trench Retreat

Case 1 assumed a constant trench retreat rate of 16 cm/yr from 15 Ma, resulting in significant trench migration. Historical retreat rate may be lower. To explore this, Cases 4 and 5 incorporated temporally varying retreat rates. Case 4 began with a retreat rate of 0 cm/yr at 15 Ma, progressively increasing to 16 cm/yr by 0 Ma. While this case still produced a slab kink around 300 km with a deepening dip angle (Figure 3a), it lacked the flat slab segment as observed and in Case 1 (Figures 2a and 2b). A flattened slab segment near 670 km was present, though shorter than in Case 1 or observations. Instead, the modeled slab geometry in Case 4 closely resembles that of Case 2 (Figure 2d), which has a constant 8 cm/yr retreat. In these two cases, the cumulated amount of trench retreat is the

same. We suggest that the amount trench retreat within a certain time span is more important than the retreat rate for slab geometry.

Case 5 (Figure 3b) incorporated a more moderate historical retreat rate, starting at 8 cm/yr at 15 Ma and reaching 16 cm/yr at 0 Ma. This case yielded a very similar slab morphology in the upper mantle compared to Case 1, including the flat segment marking a transition in dip angle (Figures 2b and 3b). The flattened slab segment near 670 km depth is also reproduced but shorter. These simulations demonstrate that an increasing trench retreat rate from 15 Ma is a viable explanation for the observed slab morphology. Furthermore, achieving a flattened slab length consistent with tomographic data likely requires a relatively fast average retreat rate during this period.

3.3. The Role of Overriding Plate Dynamics

The Tonga-Kermadec subduction zone presents a complex overriding plate (Figure 1a). The Australian Plate motion is northward while the Tonga slab subduction is westward. This allows us to consider the far western portion of the Australian Plate as stationary in a 2D model. In our reference model (Case 1), we applied a stationary tail of the Australian Plate on the western boundary (Movie S1). High strain rates induced by trench retreat and mantle flow caused localized stresses to exceed the yield stress, leading to weakening of the overriding plate. To explore the impact of overriding plate dynamics on slab geometry and back-arc basin development, we conducted two additional simulations.

In Case 6 (Figure 3c) we implemented a free-trailing Australian Plate (Movie S2). The resulting rapid eastward migration of the overriding plate, driven by mantle flow, prevented back-arc basin formation. The Tonga slab remained attached to the overriding plate, producing an unrealistic geometry. This suggests that the boundary condition in Case 1 is important to represent the Australian Plate migration for accurately modeling this subduction zone.

Case 7 (Figure 3d) investigated the effects of a non-deformable Australian Plate by imposing a no-slip surface velocity boundary condition (Movie S3). This configuration resulted in vigorous asthenospheric flow, comparable to the scenario with a free-slip Australian Plate (Figure 2b), driven by the rollback of the Tonga slab. This case has several discrepancies when compared to observations. The Lau Basin reached a width exceeding 3,000 km, significantly larger than observations. This unrealistic basin width, in turn, influenced mantle wedge flow, leading to a shallower slab dip angle above 400 km depth. The modeled slab also exhibited a lack of the characteristic flat slab segment. These outcomes highlight the critical importance of a deformable Australian Plate model for accurately capturing the dynamics of this subduction zone. The interplay between trench retreat rate, overriding plate behavior, and their combined influence is crucial for shaping the Tonga-Kermadec slab.

3.4. Opening of the Lau Basin and Thinning of the South Fiji Basin

Our model setup allows for horizontal deformation of the Lau Basin, SFB, and Zealandia lithosphere and provides insight into how extension is partitioned within the coupled subduction system (Figure 4). However, the free-slip boundary condition applied at the model surface may not fully capture the complex shallow geodynamic interactions. The 6 km vertical model resolution limits their ability to precisely represent the observed crustal thickness variations within the basins (ranging from 6 to 12 km) and the associated deformation. This limitation necessitates using an enlarged initial crustal thickness for the SFB. Additionally, the lack of detailed data hinders our understanding of the regional lithospheric structure. Considering these constraints, our discussion will focus on: (a) Qualitative comparisons of large-scale features of the modeled lithosphere with the observed crustal features (Figures 1 and 4a and 4b). (b) Quantitative evaluation of the modeled topography evolution (Figure 4c).

In Case 1, Lau Basin opened early in the evolution, reaching a width of 200 km by 12 Ma. The basin continued widening to a maximum of 800 km between 12 Ma and 6 Ma. A slight decrease in width to 700 km occurred between 6 Ma and the present (Figure 4b). Case 5 exhibited a different pattern of continuous Lau Basin widening over time (Figure 4a) while also successfully reproducing the observed slab geometry (Figure 3b). This difference highlights the primary role of trench retreat rate in controlling the basin opening process.

Cases 1 and 5 reveal a coupled process of elongation and thinning within the Australian Plate in response to trench retreat. The SFB undergoes significant thinning driven by rapid eastward asthenospheric flow (Figures 2b and 4). This thinning is most pronounced in the western part, where the lithospheric thickness decreases from 127 to ~82 km, and the crust is thinned from 38 to ~25 km (Figure S2 in Supporting Information S1). The consistent

10.1029/2024GL110127

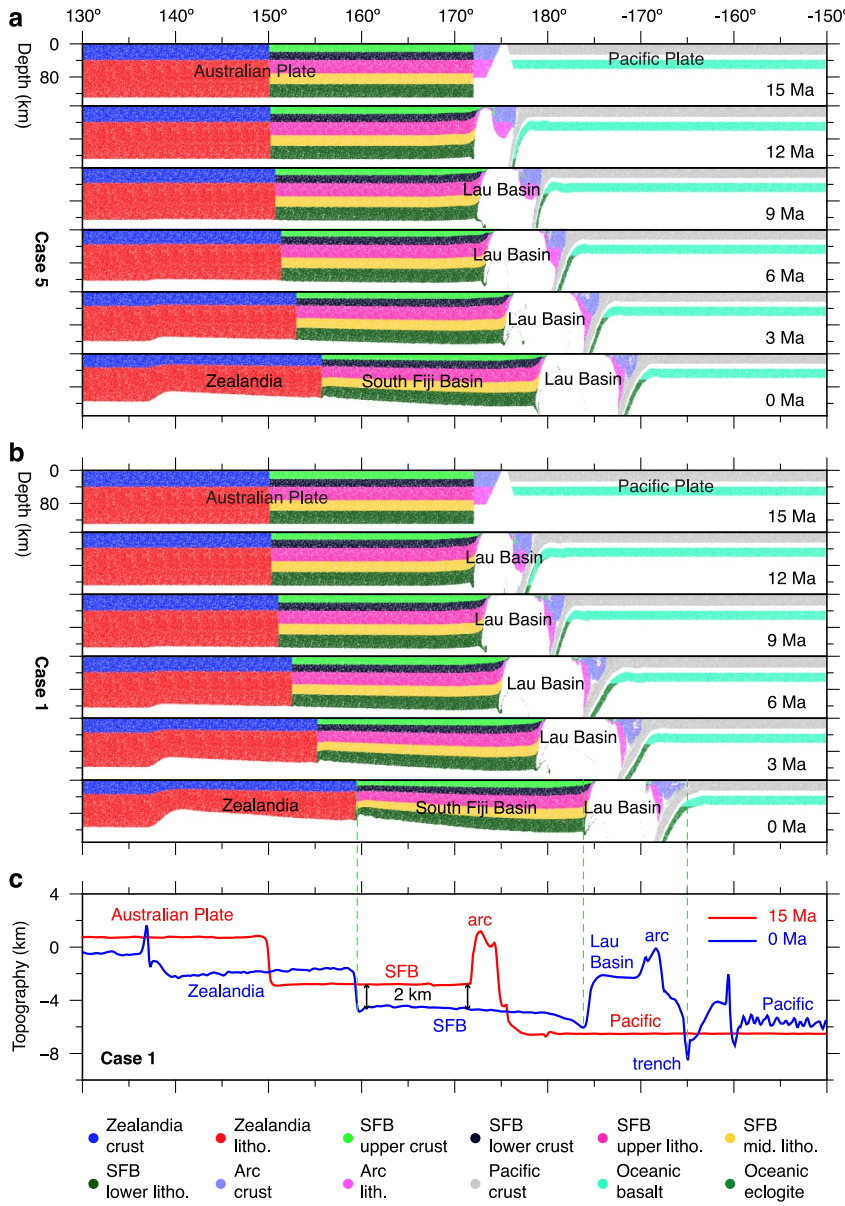

Figure 4. Lau Basin opening and SFB thinning. (a, b) Time evolution (from 15 Ma to present) of tracers within top 150 km of Cases 5 and 1, illustrating the opening of the Lau Basin, progressive thinning of SFB and Zealandia. Note that we adopted an increased initial crustal thickness for the SFB. Colored dots at the bottom legend correspond to the tracer compositions. (c) Comparison of model topography at 15 Ma (red line and texts) and present day (blue line and texts) for Case 1. The vertical black bars with arrowheads indicate the 2 km subsidence of the SFB.

35% thinning throughout the lithosphere infers that the actual SFB crust would also experience a 35% reduction, which aligns well with the difference in crustal thickness between the SFB and the Lau Basin/NFB documented in Crust 1.0 (Figures 1d–1f). Additionally, a localized deep crustal and lithospheric root develops at the intersection between Zealandia and SFB, potentially representing the Norfolk Ridge (Figures 2d and 2f).

To achieve a more accurate representation of present-day topography (Figure 4c, Figure S3 in Supporting Information S1), we iteratively refined the model building on the results from Case 1 (detailed in Supporting Information S1). The model (Figure 4c) successfully reproduces key observed features (Figures 1a and 1d–1f) for the Pacific Ocean (−5,000 to −6,000 m), Lau Basin (∼−2,200 m), SFB (∼−4,500 m), Zealandia (∼−2,000 m), Tonga Trench (∼−8,000 m), and Tonga Arc (∼0 m). Specifically for the SFB, the model suggests a subsidence of approximately 2 km over the past 15 My, which aligns well with the observed difference in bathymetry between

the SFB and the Lau Basin/NFB. We suggest that this subsidence is likely a consequence of the crustal and lithospheric thinning and may explain the deeper bathymetry of SFB compared to neighboring basins.

4. Discussion

Our modeling results show that a constant trench retreat at 16 cm/yr from 15 Ma (Case 1) can generate a Lau Basin comparable to observations. This challenges the existing view that seafloor spreading in the Lau Basin initiated ∼6 Ma (Caratori Tontini et al., 2019; Mann & Taira, 2004; Ruellan et al., 2003; Sdrolias & Müller, 2006; Taylor et al., 1996). Given a retreat rate of 16 cm/year, the Lau Basin width closely resembles the observed after 6 My of subduction (9 Ma in Case 1, see Figure 4 and Movie S1). However, the slab geometry is incorrect (Movie S1). We propose an alternative hypothesis to explain the formation of the Lau Basin, by the eastward migration of the Lau Ridge concurrent with Tonga trench retreat. Despite a trench retreat distance of about 2,000 km in the model, the eastward migration of the Lau Ridge reconciles this with the observed 700 km width (Figure 4). The Lau Basin crust exhibits westward thickening, increasing from approximately 6 km in the east (typical oceanic crust) to 9 km in the west (Crawford et al., 2003). This 50% thickening may be a direct consequence of the Lau Ridge migration which shortened the Lau Basin crust from the west.

Our hypothesis hinges on the coeval extension and thinning of the SFB and Zealandia (Figure 4). As demonstrated in Case 7 (Movie S3), assuming a rigid Australian Plate prevents the model from replicating the observed geometry of the subducting Tonga slab at any point in time. This strongly suggests that the rapid trench retreat and associated rollback of the Tonga slab must be accompanied by vigorous mantle flow within the asthenosphere. Consequently, the SFB and Zealandia are unlikely to have remained rigid throughout this process. Therefore, we propose that subsequent to the SFB's formation prior to 15 Ma, it experienced lithospheric thinning due to the mantle flow induced by Tonga slab rollback.

The SFB exhibits a bathymetry ∼2 km deeper than its neighboring basins (Figure 1a). This depth difference cannot be solely attributed to its older seafloor (10 My older than NFB and 15 My older than Lau Basin). Our models suggest lithospheric and crustal thinning as an additional contributing factor. Importantly, this process differs from typical seafloor spreading that creates younger basalts. Due to its relatively thick remaining lithosphere (over 82 km) compared to seafloor spreading centers, the SFB lacks significant recent volcanic activity.

Reconstructing past plate motion in complex regions like the Tonga-Kermadec system is challenging due to limited data and uncertainties regarding the timing and location of the trenches. Significant discrepancies exist in past plate positions (Müller et al., 2016, 2016, 2022; Seton et al., 2012; Torsvik et al., 2019), such as the location of the Tonga-Kermadec trench at 15 Ma (Figure 1c). Our models suggest eastward Lau Ridge migration, implying a larger trench retreat than previously estimated. Plate reconstructions in this region should be revisited to account for the extension within Zealandia and SFB.

A potential discrepancy exists between our hypothesis and GPS data suggesting limited recent Lau Ridge motion with respective to Australia (Bevis et al., 1995). This might be explained by the locations of the GPS sites. Situated between the New Hebrides and Tonga subduction zones (Figure 1a), these sites could be experiencing a balance of forces from both slabs, resulting in minimal net movement. Further investigation is necessary to reconcile this observation with our hypothesis. Newer, more extensive GPS measurements along the entire Lau Ridge, from north to south, could provide a clearer picture of present-day motion. Additionally, incorporating both the New Hebrides and Tonga slabs into a 3D geodynamic model would allow for a more comprehensive understanding of the regional tectonic forces.

5. Conclusion

Our 2D mantle convection models, employing a hybrid surface velocity boundary condition, reveal novel insights into the Tonga-Kermadec subduction zone. Results demonstrate that trench retreat rate is the dominant factor controlling both slab geometry and back-arc basin opening.

Challenging the traditional view of a stationary Lau-Colville Ridge relative to the Australian Plate, we propose a dynamic model where the width of the Lau Basin is determined by the eastward migration of both the Tonga and Lau Ridges. This accommodates the discrepancy between the significant magnitude of Tonga trench retreat and the comparatively smaller observed width of the Lau Basin.

Moreover, our findings indicate that the South Fiji Basin, after its formation, has experienced subsidence due to progressive lithospheric thinning driven by slab rollback. These results necessitate a reexamination of the plate motion history of the southwestern Pacific.

Data Availability Statement

The figures are plotted with GMT (https://www.generic-mapping-tools.org/). The finite element code CitcomS is available at https://geodynamics.org/resources/citcoms/ (Moresi et al., 2014). The P wave tomography model GAP-P4 is available at http://136.144.177.195/models/GAP-P4.tar.gz. Crust 1.0 is available at https://igppweb.ucsd.edu/~gabi/crust1.html. The model input parameters and output files are available at Zenodo via DOI:10.5281/zenodo.12626942 (Peng, 2024).

Acknowledgments
The authors gratefully acknowledge support from the National Science Foundation (NSF) Award 1928970. D.P. thank the Green Foundation for their support. We acknowledge the HPC resources provided by the Frontera computing project at the Texas Advanced Computing Center (TACC) made possible by National Science Foundation award OAC-1818253.

References

Artemieva, I. M. (2023). Back-arc basins: A global view from geophysical synthesis and analysis. *Earth-Science Reviews*, *236*, 104242. https://doi.org/10.1016/j.earscirev.2022.104242

Bassett, D., Kopp, H., Sutherland, R., Henrys, S., Watts, A. B., Timm, C., et al. (2016). Crustal structure of the Kermadec arc from MANGO seismic refraction profiles. *Journal of Geophysical Research: Solid Earth*, *121*(10), 7514–7546. https://doi.org/10.1002/2016JB013194

Bevis, M., Taylor, F. W., Schutz, B. E., Recy, J., Isacks, B. L., Helu, S., et al. (1995). Geodetic observations of very rapid convergence and back-arc extension at the Tonga arc. *Nature*, *374*(6519), 249–251. https://doi.org/10.1038/374249a0

Billen, M. I., & Hirth, G. (2007). Rheologic controls on slab dynamics. *Geochemistry, Geophysics, Geosystems*, *8*(8), 2007GC001597. https://doi.org/10.1029/2007GC001597

Bird, P. (2003). An updated digital model of plate boundaries. *Geochemistry, Geophysics, Geosystems*, *4*(3), 2001GC000252. https://doi.org/10.1029/2001GC000252

Caratori Tontini, F., Bassett, D., De Ronde, C. E. J., Timm, C., & Wysoczanski, R. (2019). Early evolution of a young back-arc basin in the Havre Trough. *Nature Geoscience*, *12*(10), 856–862. https://doi.org/10.1038/s41561-019-0439-y

Christensen, U. R. (1996). The influence of trench migration on slab penetration into the lower mantle. *Earth and Planetary Science Letters*, *140*(1–4), 27–39. https://doi.org/10.1016/0012-821X(96)00023-4

Conder, J. A., & Wiens, D. A. (2006). Seismic structure beneath the Tonga arc and Lau back-arc basin determined from joint Vp, Vp/Vs tomography. *Geochemistry, Geophysics, Geosystems*, *7*(3), 2005GC001113. https://doi.org/10.1029/2005GC001113

Crawford, W. C., Hildebrand, J. A., Dorman, L. M., Webb, S. C., & Wiens, D. A. (2003). Tonga Ridge and Lau Basin crustal structure from seismic refraction data. *Journal of Geophysical Research*, *108*(B4), 2001JB001435. https://doi.org/10.1029/2001JB001435

Ekström, G., Nettles, M., & Dziewoński, A. M. (2012). The global CMT project 2004–2010: Centroid-moment tensors for 13,017 earthquakes. *Physics of the Earth and Planetary Interiors*, *200–201*, 1–9. https://doi.org/10.1016/j.pepi.2012.04.002

Gill, J. B. (1976). Composition and age of Lau Basin and Ridge volcanic rocks: Implications for evolution of an Interarc basin and remnant arc. *GSA Bulletin*, *87*(10), 1384–1395. https://doi.org/10.1130/0016-7606(1976)87%3C1384:CAAOLB%3E2.0.CO;2

Hall, R. (2002). Cenozoic geological and plate tectonic evolution of SE Asia and the SW Pacific: Computer-based reconstructions, model and animations. *Journal of Asian Earth Sciences*, *20*(4), 353–431. https://doi.org/10.1016/S1367-9120(01)00069-4

Hayes, G. P., Moore, G. L., Portner, D. E., Hearne, M., Flamme, H., Furtney, M., & Smoczyk, G. M. (2018). SLAB2, a comprehensive subduction zone geometry model. *Science*, *362*(6410), 58–61. https://doi.org/10.1126/science.aat4723

Herzer, R. H., Barker, D. H. N., Roest, W. R., & Mortimer, N. (2011). Oligocene-Miocene spreading history of the northern south Fiji Basin and implications for the evolution of the New Zealand plate boundary: back-arc spreading south Fiji basin. *Geochemistry, Geophysics, Geosystems*, *12*(2). https://doi.org/10.1029/2010GC003291

Heuret, A., & Lallemand, S. (2005). Plate motions, slab dynamics and back-arc deformation. *Physics of the Earth and Planetary Interiors*, *149*(1–2), 31–51. https://doi.org/10.1016/j.pepi.2004.08.022

Kisimoto, K., Tanahashi, M., & Auzende, J.-M. (1994). Crustal structure variation along the central rift/ridge axis in the North Fiji Basin: Implications from seismic reflection and refraction data. *Marine Geology*, *116*(1–2), 101–111. https://doi.org/10.1016/0025-3227(94)90171-6

Mann, P., & Taira, A. (2004). Global tectonic significance of the Solomon Islands and Ontong Java Plateau convergent zone. *Tectonophysics*, *389*(3–4), 137–190. https://doi.org/10.1016/j.tecto.2003.10.024

McNamara, A. K., & Zhong, S. (2004). Thermochemical structures within a spherical mantle: Superplumes or piles? *Journal of Geophysical Research*, *109*(B7), 2003JB002847. https://doi.org/10.1029/2003JB002847

Moresi, L., Zhong, S., Han, L., Conrad, C., Tan, E., Gurnis, M., et al. (2014). CitcomS v3.3.1 (v3.3.1) [Software]. *Zenodo*. https://doi.org/10.5281/zenodo.7271920

Mortimer, N., Gans, P. B., Palin, J. M., Meffre, S., Herzer, R. H., & Skinner, D. N. B. (2010). Location and migration of Miocene–Quaternary volcanic arcs in the SW Pacific region. *Journal of Volcanology and Geothermal Research*, *190*(1–2), 1–10. https://doi.org/10.1016/j.jvolgeores.2009.02.017

Müller, R. D., Flament, N., Cannon, J., Tetley, M. G., Williams, S. E., Cao, X., et al. (2022). A tectonic-rules-based mantle reference frame since 1 billion years ago – Implications for supercontinent cycles and plate–mantle system evolution. *Solid Earth*, *13*(7), 1127–1159. https://doi.org/10.5194/se-13-1127-2022

Müller, R. D., Seton, M., Zahirovic, S., Williams, S. E., Matthews, K. J., Wright, N. M., et al. (2016). Ocean basin evolution and global-scale plate reorganization events since Pangea breakup. *Annual Review of Earth and Planetary Sciences*, *44*(1), 107–138. https://doi.org/10.1146/annurev-earth-060115-012211

Obayashi, M., Yoshimitsu, J., Nolet, G., Fukao, Y., Shiobara, H., Sugioka, H., et al. (2013). Finite frequency whole mantle *P* wave tomography: Improvement of subducted slab images. *Geophysical Research Letters*, *40*(21), 5652–5657. https://doi.org/10.1002/2013GL057401

Parson, L. M., Pearce, J. A., Murton, B. J., & Hodkinson, R. A. (1990). Role of ridge jumps and ridge propagation in the tectonic evolution of the Lau back-arc basin, southwest Pacific. *Geology*, *18*(5), 470. https://doi.org/10.1130/0091-7613(1990)018<0470:RORJAR>2.3.CO;2

Peng, D. (2024). Parameters and results of 2D Tonga subduction models [Dataset]. *Zenodo*. https://doi.org/10.5281/zenodo.12626942

Peng, D., & Stegman, D. R. (2024). Modeling subduction with extremely fast trench retreat. *ESS Open Archive*. https://doi.org/10.22541/essoar.171288715.53824453/v1

Richards, S., Holm, R., & Barber, G. (2011). When slabs collide: A tectonic assessment of deep earthquakes in the Tonga-Vanuatu region. *Geology*, *39*(8), 787–790. https://doi.org/10.1130/G31937.1

Ruellan, E., Delteil, J., Wright, I., & Matsumoto, T. (2003). From rifting to active spreading in the Lau Basin – Havre Trough backarc system (SW Pacific): Locking/unlocking induced by seamount chain subduction. *Geochemistry, Geophysics, Geosystems*, *4*(5), 2001GC000261. https://doi.org/10.1029/2001GC000261

Schellart, W. P., Freeman, J., Stegman, D. R., Moresi, L., & May, D. (2007). Evolution and diversity of subduction zones controlled by slab width. *Nature*, *446*(7133), 308–311. https://doi.org/10.1038/nature05615

Sdrolias, M., & Müller, R. D. (2006). Controls on back-arc basin formation. *Geochemistry, Geophysics, Geosystems*, *7*(4), 2005GC001090. https://doi.org/10.1029/2005GC001090

Seton, M., Müller, R. D., Zahirovic, S., Gaina, C., Torsvik, T., Shephard, G., et al. (2012). Global continental and ocean basin reconstructions since 200Ma. *Earth-Science Reviews*, *113*(3–4), 212–270. https://doi.org/10.1016/j.earscirev.2012.03.002

Seton, M., Müller, R. D., Zahirovic, S., Williams, S., Wright, N. M., Cannon, J., et al. (2020). A global data set of present-day oceanic crustal age and seafloor spreading parameters. *Geochemistry, Geophysics, Geosystems*, *21*(10), e2020GC009214. https://doi.org/10.1029/2020GC009214

Shor, G. G., Kirk, H. K., & Menard, H. W. (1971). Crustal structure of the Melanesian area. *Journal of Geophysical Research*, *76*(11), 2562–2586. https://doi.org/10.1029/JB076i011p02562

Stewart, M. S., Hannington, M. D., Emberley, J., Baxter, A. T., Krätschell, A., Petersen, S., et al. (2022). A new geological map of the Lau Basin (southwestern Pacific Ocean) reveals crustal growth processes in arc-backarc systems. *Geosphere*. https://doi.org/10.1130/GES02340.1

Tan, E., & Gurnis, M. (2007). Compressible thermochemical convection and application to lower mantle structures. *Journal of Geophysical Research*, *112*(B6), 2006JB004505. https://doi.org/10.1029/2006JB004505

Taylor, B., Zellmer, K., Martinez, F., & Goodliffe, A. (1996). Sea-floor spreading in the Lau back-arc basin. *Earth and Planetary Science Letters*, *144*(1–2), 35–40. https://doi.org/10.1016/0012-821X(96)00148-3

Torsvik, T. H., Steinberger, B., Shephard, G. E., Doubrovine, P. V., Gaina, C., Domeier, M., et al. (2019). Pacific-Panthalassic reconstructions: Overview, errata and the way forward. *Geochemistry, Geophysics, Geosystems*, *20*(7), 3659–3689. https://doi.org/10.1029/2019GC008402

Van De Lagemaat, S. H. A., & Van Hinsbergen, D. J. J. (2024). Plate tectonic cross-roads: Reconstructing the Panthalassa-Neotethys junction region from Philippine Sea Plate and Australasian oceans and Orogens. *Gondwana Research*, *126*, 129–201. https://doi.org/10.1016/j.gr.2023.09.013

Wallace, L. M., McCaffrey, R., Beavan, J., & Ellis, S. (2005). Rapid microplate rotations and backarc rifting at the transition between collision and subduction. *Geology*, *33*(11), 857. https://doi.org/10.1130/G21834.1

Zellmer, K. E., & Taylor, B. (2001). A three-plate kinematic model for Lau Basin opening. *Geochemistry, Geophysics, Geosystems*, *2*(5), 2000GC000106. https://doi.org/10.1029/2000GC000106

Zhong, S., Zuber, M. T., Moresi, L., & Gurnis, M. (2000). Role of temperature-dependent viscosity and surface plates in spherical shell models of mantle convection. *Journal of Geophysical Research*, *105*(B5), 11063–11082. https://doi.org/10.1029/2000JB900003

References From the Supporting Information

Peng, D., Liu, L., & Wang, Y. (2021a). A newly discovered late-cretaceous east Asian flat slab explains its unique lithospheric structure and tectonics. *Journal of Geophysical Research: Solid Earth*, *126*(10), e2021JB022103. https://doi.org/10.1029/2021JB022103

Peng, D., Liu, L., Hu, J., Li, S., & Liu, Y. (2021b). Formation of east Asian stagnant slabs due to a pressure-driven Cenozoic mantle wind following Mesozoic subduction. *Geophysical Research Letters*, *48*(18), e2021GL094638. https://doi.org/10.1029/2021GL094638